DALTON
FULL PAPER

Structural analysis and magnetic properties of the 1-D compounds $[M(NCS)_2bpa_2]$ [M = Fe, Co, Ni and bpa = 1,2-bis(4-pyridyl)-ethane]

Margarita L. Hernández,[a] M. Gotzone Barandika,[a,b] M. Karmele Urtiaga,[c] Roberto Cortés,[b] Luis Lezama,[a] M. Isabel Arriortua[c] and Teófilo Rojo *[a]

[a] *Departamento de Química Inorgánica, Facultad de Ciencias, Universidad del País Vasco, Apdo. 644, Bilbao 48080, Spain. E-mail: qiproapt@lg.ehu.es*
[b] *Departamento de Química Inorgánica, Facultad de Farmacia, Universidad del País Vasco, Apdo. 450, Vitoria 01080, Spain*
[c] *Departamento de Mineralogía-Petrología, Facultad de Ciencias, Universidad del País Vasco, Apdo. 644, Bilbao 48080, Spain*

Received 5th January 1999, Accepted 11th March 1999

The increasing interest in designing polymeric compounds has focused this work on the synthesis and magnetostructural characterization of three 1-D compounds of general formula $[M(NCS)_2bpa_2]$ [M = Fe, Co, Ni and bpa = 1,2-bis(4-pyridyl)ethane] which exhibit double bpa bridges between metallic cations. X-Ray single crystal diffraction analysis was carried out on **1** $[Fe(NCS)_2bpa_2]$ while for **2** $[Co(NCS)_2bpa_2]$ and **3** $[Ni(NCS)_2bpa_2]$ the structural characterization was performed on powdered samples. UV-VIS results were consistent with high-spin metallic cations in tetragonally distorted octahedral fields. Although in the three compounds weak antiferromagnetic coupling has been observed taking place through the $–M–(bpa)_2–M–$ bridges, for the theoretical analysis of the global magnetic behaviour of all of them some other effects have been considered, *i.e.* zero field splitting and spin–orbit coupling.

Introduction

Over the last few years, the design of polymeric compounds has been an active area of research in coordination chemistry. So far, extended systems of a variety of metals and ligands have been characterized providing very interesting information about magnetostructural co-relations in these compounds.[1,2]

The generation of this type of molecular architecture rests on the combination of several factors like the coordination geometry of the metals, the performance of the ligands and the reaction conditions. In relation to the ligands, the use of pseudo-halides and voluminous organic molecules has been well established and results in covalent high-dimensional arrangements. While the role of ambidentate pseudo-halides is clearly related to their ability to form interaction bridges, the function of the voluminous ligands has been mainly linked to their coordination-site-blocking behaviour.[3,4] However, the bridging capability exhibited by several polydentate organic molecules enhances the possibility of generating high-dimensional systems. Compounds obtained by using N,N′ bidentate spacers[5–11] like 4,4′-bipyridine, pyrazine and other related ligands are illustrative of this point.

For a self-assembly strategy of the synthesis of these compounds, the rigidity of the aforementioned ligands is clearly a limiting factor. Therefore, the use of flexible linkers represents an excellent alternative for further research. Among them, 1,2-bis(4-pyridyl)ethane has been used to this purpose in several recent works.[12,13] This ligand has been observed to exhibit two different conformations, *anti* and *gauche* (Scheme 1), being remarkably versatile as a spacer in extended systems.[14] Thus, isomerism and its manifestation in the structure have become issues which demand much work in this area.

Taking into account the aforementioned aspects, three compounds of formula $[M(NCS)_2bpa_2]$ [M = Fe **1**, Co **2** and Ni **3** and bpa = 1,2-bis(4-pyridyl)ethane] were prepared in order to study the influence of both ligands in the structure and magnetic properties of the 1-D systems obtained.

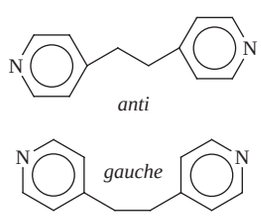

Scheme 1

Experimental

Synthesis

Synthesis of compound **1** (yield 63%) was carried out by mixing an ethanolic solution of $FeCl_2·4H_2O$ (0.5 mmol, 25 ml) also containing an excess of NaNCS with a methanolic solution of bpa (1 mmol, 25 ml). This solution was left to stand at room temperature. After several days, prismatic, yellow, X-ray quality single crystals were obtained.

Synthesis of compound **2** (yield 82%) was performed by mixing an ethanolic solution of $Co(CH_3CO_2)_2·4H_2O$ (0.5 mmol, 25 ml) with a methanolic solution (25 ml) containing bpa (1.0 mmol) and NaNCS (2.5 mmol) resulting in a red precipitate. Compound **3** (yield 80%) was also obtained as a precipitate (light blue coloured) after following the procedure for compound **2** with $NiCl_2·6H_2O$. Further attempts to recrystallize these precipitates in several mixtures of ethanol, methanol, acetone and water gave rise to poor quality single crystals.

Elemental analysis and atomic absorption results were in good agreement with the $MC_{26}N_6H_{24}S_2$ (M = Fe, Co, Ni) stoichiometry for the three compounds. Found (calc.)%: Fe,

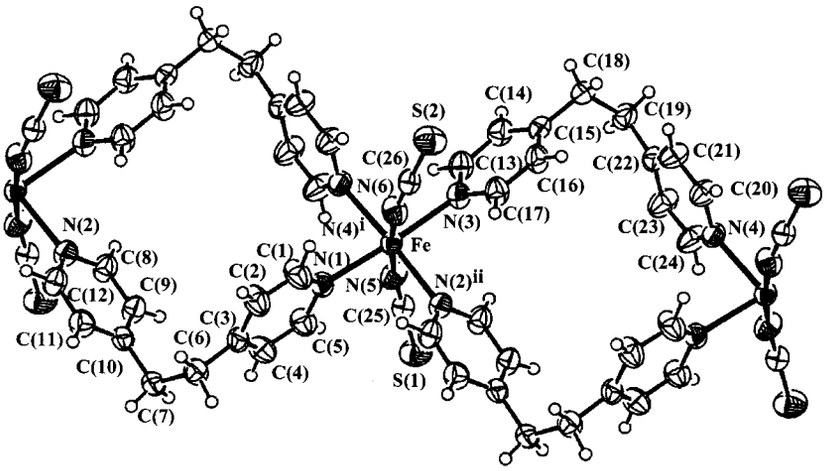

Fig. 1 ORTEP[33] view (50% probability) of the linear chains extending along the [010] direction for $[Fe(NCS)_2bpa_2]$ **1**.

Table 1 Crystal data and structure refinement for compound **1**

Formula	$Fe_{0.5}C_{13}N_3SH_{12}$	T/°C	20
M	270.24	λ/Å[a]	0.71070
Space group	$C2/c$	ρ_{obs}/g cm^{-3}	1.33(2)
a/Å	19.077(4)	ρ_{calc}/g cm^{-3}	1.375
b/Å	9.995(3)	μ/cm^{-1}	7.64
c/Å	14.588(4)	Unique data	3940
β/°	110.23(3)	Observed data	3168
U/Å^3	2610(1)	$R(R')$[b]	0.0355(0.0927)
Z	8		

[a] Mo-Kα radiation, graphite monochromator. [b] $R = [\Sigma||F_o| - |F_c||/\Sigma|F_o|]$, $R' = \{\Sigma[w(F_o^2 - F_c^2)^2]/\Sigma[w(F_o^2)^2]\}^{\frac{1}{2}}$ where $w = 1/\sigma^2(|F_o|)$.

10.43 (10.34); S, 11.53 (11.87); N, 16.01 (15.56); C, 58.07 (57.76); H, 4.27 (4.47) for **1**: Co, 11.10 (10.85); S, 11.61 (11.77); N, 15.56 (15.47), C, 57.36 (57.45); H, 4.24 (4.45) for **2**: Ni, 11.10 (10.80); S, 11.68 (11.80); N, 15.58 (15.47), C, 57.74 (57.48); H, 4.21 (4.45) for **3**.

TG curves obtained for compounds **1**, **2** and **3** (25–500 °C) showed that, as reported for similar compounds,[15] the three of them undergo pyrolysis of the ligands taking place in two steps. The first of them, being centred at 275 °C, can be attributed to the loss of a molecule of bpa per formula unit while the second one takes place at around 425 °C. The identification of the final residues through X-ray diffraction was not possible due to the low crystallinity of the samples.

Physical measurements

Microanalyses were performed with a Perkin-Elmer 2400 analyser. Analytical measurements were carried out in an ARL 3410 + ICP with Minitorch equipment. IR spectroscopy was performed on a Nicolet 520 FTIR spectrophotometer in the 400–4000 cm^{-1} region. Diffuse reflectance spectra were registered at room temperature on a CARY 2415 spectrometer in the range 5000–45000 cm^{-1}. TG curves were obtained using a Perkin-Elmer System-7 DSC-TGA unit at a heating rate of 5 °C min^{-1} in nitrogen. ESR spectroscopy was performed on powdered samples at X frequency, with a Bruker ESR 300 spectrometer, equipped with a standard Oxford low-temperature device, calibrated by the NMR probe for the magnetic field, the frequency being measured by using a Hewlett-Packard 5352B microwave frequency computer. Magnetic susceptibilities of powdered samples were carried out in the temperature range 1.8–300 K using a Quantum Design Squid magnetometer, equipped with a helium continuous-flow cryostat. The magnetic field was approximately 1000 G, a field at which the magnetisation *versus* magnetic field curve is linear even at 1.8 K. The experimental susceptibilities were corrected for diamagnetism of the constituent atoms (Pascal tables).

Table 2 Structural data and refinement for compounds **2** and **3**

Compound	**2**	**3**
Formula	$Co_{0.5}C_{13}N_3SH_{12}$	$Ni_{0.5}C_{13}N_3SH_{12}$
M	271.66	271.55
Space group	$C2/c$	$C2/c$
a/Å	19.762(1)	19.7841(7)
b/Å	9.9430(7)	9.8630(6)
c/Å	14.581(1)	14.5239(7)
β/°	110.388(4)	110.050(5)
U/Å^3	2685.6(1)	2662.3(7)
T/°C	25	25
λ/Å	1.5418	1.5418
R_b[a]	2.88	1.35
R_p[b]	9.19	6.27
R_{wp}[c]	12.7	8.48

[a] $R_b = 100[\Sigma|I_o - I_c|]/\Sigma|I_o|$. [b] $R_p = 100[\Sigma|y_o - y_c|]/\Sigma|y_o|$. [c] $R_{wp} = (\Sigma[w|y - y_c|^2]/\Sigma[w|y_o|^2])^{\frac{1}{2}}$.

Crystal structure determination

X-Ray measurements for compound **1** were taken at room temperature on an Enraf-Nonius CAD-4 diffractometer, operating in ω–2θ scanning mode using suitable crystals for data collection. Accurate lattice parameters were determined from least-squares refinement of 25 well-centred reflections. Intensity data were collected in the θ range 2.28–31.07°. During data collection, two standard reflections periodically observed showed no significant variation. Corrections for Lorentz and polarization factors were applied to the intensity values.

The structure was solved by heavy-atom Patterson methods using the program SHELXS86[16] and refined by a full-matrix least-squares procedure on F^2 using SHELXL93.[17] Non-hydrogen atomic scattering factors were taken from ref. 18. Crystallographic data and processing parameters for compound **1** are shown in Table 1.

CCDC reference number 186/1380.

See http://www.rsc.org/suppdata/dt/1999/1401/ for crystallographic files in .cif format.

X-Ray powder diffraction data for compounds **2** and **3** were collected on a PHILIPS X'PERT powder diffractometer with Cu-Kα radiation in steps of 0.02° (2θ) over the 5–60° (2θ) angular range and a fixed-time counting of 4 s at 25 °C. The powder diffraction pattern was indexed with the FULLPROF[19] program based on the Rietveld method[20–21] using the *Profile Matching* option. Crystallographic data and processing parameters for compounds **2** and **3** are given in Table 2.

Results and discussion

Structural analysis

The structure of $[Fe(NCS)_2bpa_2]$ complex **1** consists of linear

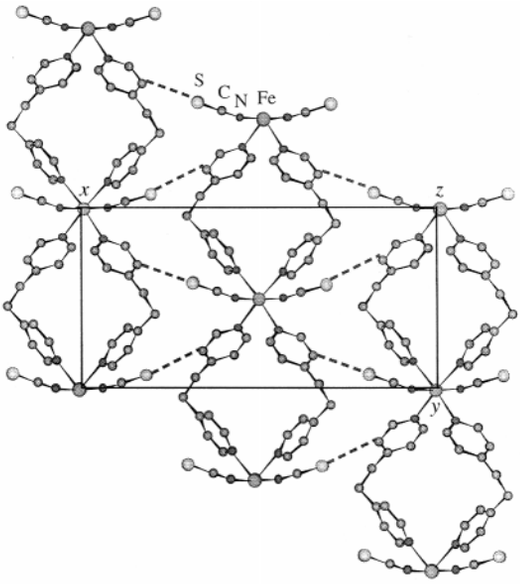

Fig. 2 View of the non-planar packing for $[Fe(NCS)_2bpa_2]$ **1**. The discontinuous lines represent interchain H-bonds.

Table 3 Selected bond distances (Å) and angles (°) for compound **1**

Fe–N1	2.220(2)	$N3^{(i)}$–Fe–N3	175.84(9)
$Fe–N2^{(ii)}$	2.222(2)	$N1^{(i)}$–Fe–N1	84.84(8)
Fe–N3	2.069(2)	$N1^{(i)}$–Fe–$N2^{(iii)}$	91.99(6)
N3–C13	1.118(2)	$N2^{(ii)}$–Fe–$N2^{(iii)}$	86.59(8)
C13–S	1.562(2)	$N3^{(i)}$–Fe–$N2^{(ii)}$	94.78(7)
		N3–C13–S	179.3(2)

Hydrogen bonds

D–H	D···A	H···A	D–H···A
C9–H9	$C9\cdots S2^{(v)}$	$H9\cdots S2^{(v)}$	$C9–H9\cdots S2^{(v)}$
0.86(2)	3.518(2)	2.79(2)	143.1(2)

Symmetry codes: (i) $-x$, y, $-z + 1/2$; (ii) x, $y + 1$, z; (iii) $-x$, $y + 1$, $-z + 1/2$; (iv) x, $y - 1$, z; (v) $x - 1/2$, $y - 1/2$, z.

chains extending along the [010] crystallographic direction (Fig. 1). Metallic Fe(II) ions are bridged through two N,N′ bidentate bpa ligands. The coordination sphere around Fe(II) is a FeN_6 octahedron in which the equatorial positions are occupied by four N_{bpa} atoms while the axial positions are occupied by terminal N-bonded isothiocyanate ligands which are nearly linear. The Fe–N_{NCS} distances [2.069(2) Å] are shorter than the Fe–N_{bpa} ones (2.221 Å, on average) giving rise to a compressed octahedral coordination sphere in which all the angles are close to the ideal ones. Table 3 summarizes the selected bond distances and angles for compound **1**.

The intrachain distance between metallic cations [9.995(3) Å] is shorter than the one found in a similar 1-D compound of Fe(II) where the metallic ions are bridged by 4,4′-bipyridine[5] as a result of the *gauche* conformation of the bpa in compound **1** [torsion angle C3–C6–C7–C10 is 68.2(3)°]. On the other hand, the Fe–Fe interchain distance along the z axis in compound **1** [7.292(2) Å] is shorter than the intrachain distance as the chains are connected through hydrogen bonds between S_{NCS} atoms and the pyridyl rings (Table 3). The resulting 2-D network of non-planar layers can be seen in Fig. 2, the Fe–Fe interchain distance being 10.768(4) Å.

X-Ray diffraction patterns for compounds **2** and **3** are very similar to the theoretical pattern generated for compound **1**. Therefore, the values corresponding to the cell parameters and space group of compound **1** were used as initial data for the refinement of the experimental patterns for compounds **2** and **3**. The experimental, calculated (according to the best fit parameters shown in Table 2) and difference patterns are shown

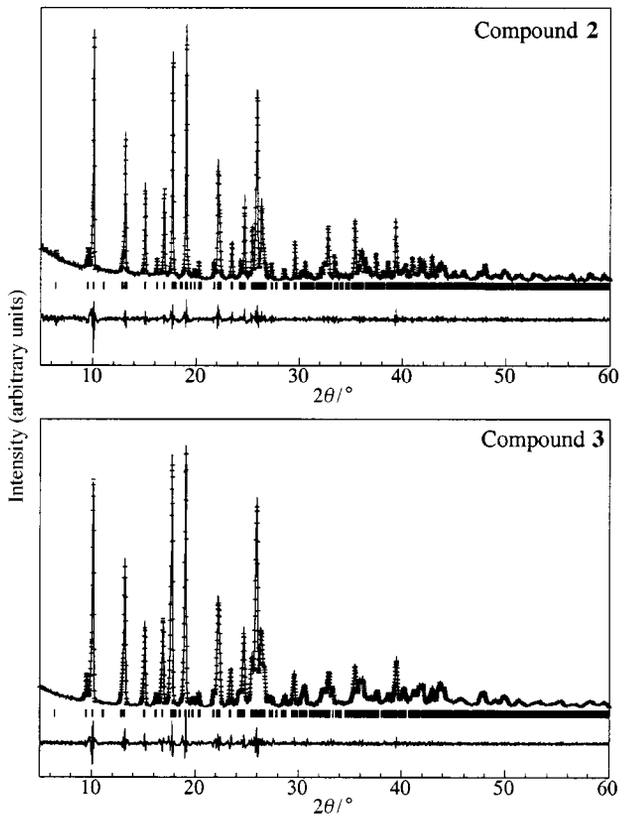

Fig. 3 Experimental, calculated and difference powder X-ray diffraction patterns for (top) $[Co(NCS)_2bpa_2]$ **2** and (bottom) $[Ni(NCS)_2bpa_2]$ **3**.

in Fig. 3 for compounds **2** and **3**. These results clearly indicate that compounds **1**, **2** and **3** are isomorphous.

IR and UV-VIS spectroscopies

It is worth mentioning that the major application of IR spectroscopy in pseudo-halide containing compounds is usually focused on the bands corresponding to these ambidentate ligands as they can provide very useful information about the pseudo-halide coordination mode. In particular, for N-bonded isothiocyanate, the most intense band appears at about 2050 cm^{-1} being related to the asymmetric streching mode of the C=N bond, while for S-bonded thiocyanate, this band can be found at about 2100 cm^{-1}. Thus, for N,S-bonded thiocyanate, this absorption appears as a split band in the vicinity of these values.

A summary of the most important IR bands corresponding to compounds **1**, **2** and **3** together with their tentative assignments is given in Table 4. As can be observed, the three IR spectra show an intense single band at about 2065 cm^{-1} which is associated with the ν_{asym} streching mode of the C=N bond of N-coordinated isothiocyanate. On the other hand, the frequencies of the bands related to the bpa ligand in the three compounds are very close to their positions in the free ligand (which are also displayed in Table 4) indicating that the pyridyl rings are nearly planar in the complexes. These results are indicative of a similar coordination of the ligands to the metallic ions, as expected for isomorphous compounds.

The diffuse reflectance spectrum for compound **1** is typical of octahedral high spin Fe(II) complexes with Jahn–Teller distortion which specially affect the ^5e_g orbitals as a result of the shorter axial distances.[22] Thus, the spectrum shows the only spin-allowed transition $^5T_{2g}\rightarrow{}^5E_g$ split into two bands at 10810 and 19646 cm^{-1}. The corresponding value of $(8/3)d\sigma = 8836$ cm^{-1} is comparable to those calculted for Fe(II) octahedral complexes with tetradentate, conjugated, cyclic N_4-ligands.[23]

Table 4 Selected IR bands for bpa and $[Fe(NCS)_2bpa_2]$ **1**, $[Co(NCS)_2bpa_2]$ **2** and $[Ni(NCS)_2bpa_2]$ **3** together with their assignments

Compound	bpa	**1**	**2**	**3**
Thiocyanate, ν(CN)		2056i	2062i	2079i
Pyridyl ring stretching, ν(C=C)	1594i	1614m	1614m	1614m
ν(ArC–C, C=N)	1413i	1415m	1418m	1420m
Pyridyl ring breathing, δ(ArC–H)	982m	1016m	1016m	1016m
Pyridyl out of plane bending, ν(ArC–H)	817i	827m	812m	827m
Pyridyl ring in plane vibration	539i,sp	525m,sp	521m,sp	546m,sp

i = intense, m = medium, sp = split.

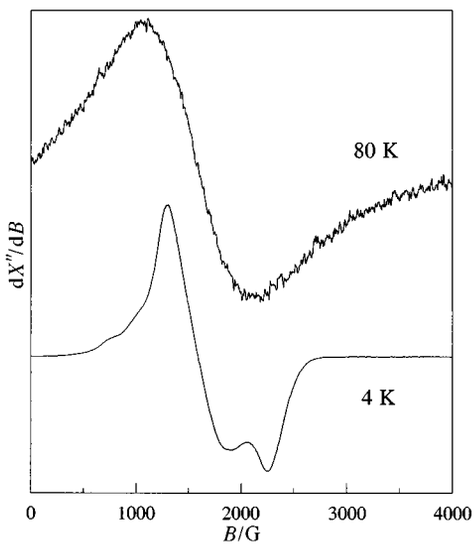

Fig. 4 X-Band ESR spectra for $[Co(NCS)_2bpa_2]$ **2** at 80 and 4 K.

Additionally, the spectrum exhibits a charge-transfer band above 21000 cm^{-1} which is in accordance with the fact that the metallic cation is surrounded by four pyridine rings.

For compound **2**, the diffuse reflectance spectrum exhibits two absorptions which have been attributed to the spin allowed transitions from $^4T_{1g}$ to $^4T_{2g}$ and $^4T_{1g}(P)$, respectively. The first absorption is split into two at 9435 and 12075 cm^{-1}, respectively, while the second is located at 20000 cm^{-1}. The split of the first transition must also be interpreted in terms of the Jahn–Teller distortion affecting the ^5e_g orbitals. The expected transition to $^4A_{2g}$ appears as a shoulder on the second transition, its position not having been measured. The values of $Dq = 1059$ cm^{-1} and $B = 795$ cm^{-1} which have been estimated from these transitions are typical for high spin Co(II) complexes.[22] The value of B is indicative of an 80% covalency of the Co–N bonds in compound **2**. This spectrum also shows a charge-transfer band above 25000 cm^{-1}.

Compound **3** exhibits two reflectance spectrum bands at 10566 and 17452 cm^{-1} which have been assigned to the spin allowed transitions from $^3A_{2g}$ to $^3T_{2g}$ and $^4T_{1g}$. According to these bands, a value of $Dq = 1057$ cm^{-1} has been calculated which is typical for Ni(II) compounds.[22] This spectrum also shows a charge-transfer band above 29000 cm^{-1} which hides the expected third transition from $^3A_{2g}$ to $^3T_{1g}(P)$.

In summary, diffuse reflectance data clearly indicate that the bpa ligand generates a low perturbation on the octahedral coordination spheres of the title compounds. Additionally, the shorter $M–N_{NCS}$ distances in the axial positions give rise to a tetragonal Jahn–Teller distortion according to which $d_{x^2-y^2}$ orbitals becomes more stable than d_{z^2} orbitals.

ESR and magnetic properties

ESR measurements were carried out at several temperatures in the range 2–300 K for compounds **1**, **2** and **3**. As expected for compounds **1** and **3**, having non-Kramer metallic ions, ESR spectra did not show any signals over the whole temperature range. For compound **2**, even if X-band isotropic spectra were recorded below 100 K, just those corresponding to temperatures lower than 40 K acquired rhombic resolution. This is illustrated in Fig. 4, where the spectra recorded at 80 and 4 K can be seen.

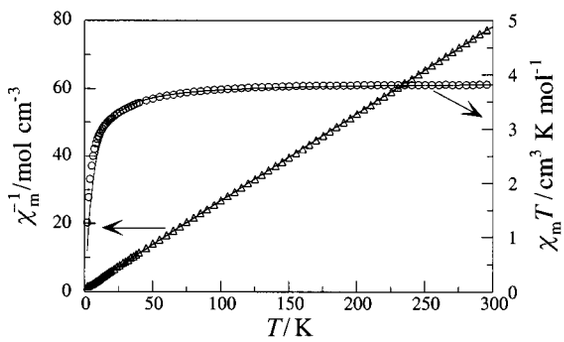

Fig. 5 Thermal evolution of χ_m^{-1} and $\chi_m T$ for $[Fe(NCS)_2bpa_2]$ **1** and their corresponding theoretical curves.

The spectrum at 4 K can be described in terms of an effective spin doublet $S = 1/2$ arising from the splitting of the $^4T_1$ term as a result of the spin–orbit coupling in octahedral Co(II). The sum of the three observed g-values, $g_1 = 5.20$, $g_2 = 4.15$ and $g_3 = 3.00$, are close to the theoretical value of 13 proposed by Abragam and Pryce[24] which is consistent with the slightly distorted octahedral sphere around Co(II) in compound **2**.

Measurement of the thermal variation of the magnetic susceptibility for compounds **1**, **2** and **3** showed that χ_m values continuously increase upon cooling for all three compounds, not exhibiting any maxima in the entire temperature range studied.

The experimental data for compound **1**, plotted as the thermal variation of the reciprocal susceptibility and the $\chi_m T$ product are shown in Fig. 5. The variation of χ_m^{-1} is well described by the Curie–Weiss law over the whole temperature range, with values of C_m and θ of 3.88 cm^3 K mol^{-1} and −3.7 K, respectively. The calculated value of g, 2.27, lies among the usual ones for octahedral Fe(II) (2.08–2.33).[25] The $\chi_m T$ term is practically constant down to 100 K, rapidly decreasing upon further cooling.

The thermal variation of $\chi_m T$ together with the sign of the Weiss constant could be consistent with the occurrence of antiferromagnetic coupling. Eqn. (1) can be proposed as a theoretical approach to the magnetic behaviour of compound **1**. In this expression, χ_m is a function of the J parameter due to exchange couplings along an infinite-spin, linear chain[26] with $S = 2$.

$$\chi_m = \frac{6Ng^2\beta^2}{3kT}\left[\frac{1-u}{1+u}\right] \quad (1)$$

where $$u = \frac{T}{T_0} - \coth\left(\frac{T}{T_0}\right) \text{ and } T_0 = 12\frac{J}{k}$$

N and k are the Avogadro and Boltzmann constants, respectively, and β is the Bohr magneton.

According to eqn. (1), the best fit parameters for compound **1** have been determined to be $g = 2.27$ and $J = -0.5$ K. The fact that the theoretical curve shows a slight discrepancy with the experimental data at very low temperatures could be indicative

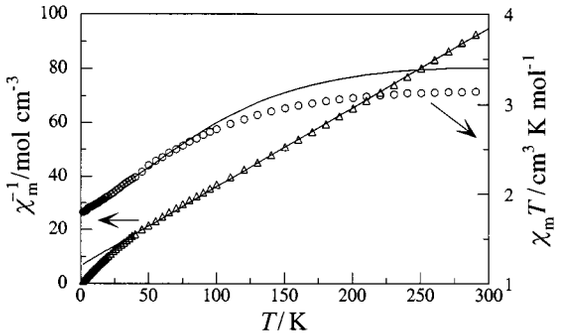

Fig. 6 Thermal evolution of χ_m^{-1} and $\chi_m T$ for $[Co(NCS)_2bpa_2]$ **2** and their corresponding theoretical curves.

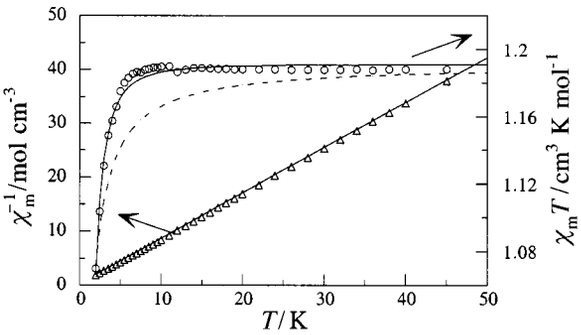

Fig. 7 Thermal evolution of χ_m^{-1} and $\chi_m T$ for $[Ni(NCS)_2bpa_2]$ **3** and their corresponding theoretical curves [continuous and discontinuous lines for $\chi_m T$ correspond to $\chi_m = f(D)$ and $\chi_m = f(J)$, respectively].

of the occurrence of a second effect in addition to the antiferromagnetic interactions. Even if the zero field splitting could be proposed to be this second effect, the occurrence of a spin transition might also be considered.

As reported elsewhere,[27,28] the N-coordinated bpa could be expected to cause a spin transition in Fe(II) systems. Obviously, the temperature required for the spin transition to occur is related to the perturbation originated by bpa on the ligand field which has been observed to be very weak. Thus, assuming that the spin transition does exist for compound **1**, it should be concluded that it takes place at around 10 K finishing at a temperature below 2 K (below the studied range). Comparison between this low temperature and the $T_{1/2}$ value of 138 K observed for $[Fe(DPEA)(NCS)_2]$[29] [DPEA = (2-aminoethyl)bis-(2-pyridylmethyl)amine] as well as the temperature range of 100–250 K attributed to the spin transition for $[Fe(tvp)_2(NCS)_2]\cdot CH_3OH$[30] [tvp = 1,2-bis(4-pyridyl)ethylene] is illustrative of the weaker ligand field force generated by bpa.

Plots of χ_m^{-1} and $\chi_m T$ *vs.* temperature are shown in Fig. 6 for compound **2**. As can be seen, the Curie–Weiss law is followed at temperatures down to 50 K, with values of C_m and θ of 3.40 cm^3 K mol^{-1} and −22.6 K, respectively. The decreasing value of $\chi_m T$ upon cooling could indicate the existence of antiferromagnetic coupling. However, the long pathway through the organic ligand as well as the high value of the Weiss constant preclude that the decrease of μ_{eff} should be mainly attributed to spin–orbit coupling.

In order to theoretically study the magnetic behaviour of compound **2**, eqn. (2) has been used.[25] This expression proposes μ_{eff} to be a function of λ (related to the spin–orbit coupling) and a (corresponding to the ligand field).

The minimum experimental value of μ_{eff}, 3.82 μ_B, coincides with the theoretical low field value for octahedral Co(II) which is due to the low perturbation generated by the bpa ligand (as concluded from diffuse reflectance spectra). Therefore, $a = 1.5$ has been considered for the fitting of eqn. (2). In this way, the best fit value for λ has been found to be −144.8 cm^{-1}. This model quite accurately reproduces the experimental data at low temperatures. The slight deviation observed at high temperatures could be caused by the anisotropy of the octahedral sphere. Additionally, the decrease in λ in relation to the value corresponding to the free ion (85%) can be attributed to the covalency of the Co–N bonds.

The thermal evolution of χ_m^{-1} for compound **3**, shown in Fig. 7, can be described by the Curie–Weiss law down to 20 K with $C_m = 1.19$ cm^3 K mol^{-1} and $\theta = -0.4$ K. The calculated value of g (2.18) is typical for octahedral Ni(II). The thermal trend exhibited by $\chi_m T$, also shown in Fig. 7, indicates a sharp decrease of μ_{eff} at temperatures below 8 K which could be associated with the occurrence of antiferromagnetic interactions and a zero field splitting effect, or a zero field splitting effect, only.

With the aim of analysing the magnetic behaviour of compound **3**, eqn. (3) and (4) have been considered. In eqn. (3),

$$\chi_m = \frac{2Ng^2\beta^2}{3kT}\left[\frac{\frac{2}{x} - \frac{2\exp(-x)}{x} - \ + \exp(-x)}{1 + 2\exp(-x)}\right] \qquad (3)$$

$$\text{where } x = \frac{D}{kT}$$

$$\chi_m = \frac{Ng^2\beta^2}{kT}\left[\frac{2 + 0.0194X + 0.777X^2}{3 + 4.346X + 3.232X^2 + 5.834X^3}\right] \qquad (4)$$

$$\text{where } X = J(kT)^{-1}$$

which corresponds to the Van Vleck equation[31] for $S = 1$, χ_m is given as a function of the zero field splitting term D. On the other hand, by means of eqn. (4), χ_m is supposed to depend on the J parameter related to the antiferromagnetic coupling in a 1-D system[32] with $S = 1$, by considering the ground term $^3A_2$ and the interactions between nearest neighbours. According to both suppositions, the best fit parameters have been found to be $g = 2.183$ and $D = 1.9$ cm^{-1} for eqn. (3) and $g = 2.182$ and $J = 0.1$ cm^{-1} for eqn. (4).

In Fig. 7 the theoretical curves obtained from eqn. (3) and (4) are shown up to 50 K. Theoretical values above this temperature have been omitted as they do not show any significant discrepancies. As can be seen, the curve corresponding to eqn. (3) [$\chi_m = f(D)$] fits the experimental data more efficiently than the curve corresponding to eqn. (4) [$\chi_m = f(J)$]. Additionally, the low value of J obtained from eqn. (4) indicates that, even if the existence of antiferromagnetic coupling should not be neglected, the effect of the zero field splitting term is more relevant for the magnetic properties of compound **3**.

Conclusions

Three polynuclear compounds were prepared using the transition metal cations Fe(II), Co(II) and Ni(II) in combination with the pseudo-halide NCS^- and the bidentate organic ligand bpa. X-Ray single crystal diffraction characterization carried

$$\mu_{eff}^2 = \frac{\frac{7(3-a)^2x}{5} + \frac{12(2+a)^2}{25a} + \left\{\frac{2(11-2a)^2x}{45} + \frac{176(2+a)^2}{675a}\right\} x\exp\left(\frac{-5ax}{2}\right) + \left\{\frac{(5+a)^2x}{9} - \frac{20(2+a)^2}{27a}\right\}\exp(-4a^x)}{\frac{x}{3}\left\{3 + 2\exp\left(\frac{-5ax}{2}\right) + \exp(-4ax)\right\}} \qquad (2)$$

where $x = \lambda(kT)^{-1}$

out on the compound with Fe(II) revealed that this compound consists of linear chains in which the metallic cations are connected through two bpa ligands in *gauche* disposition. For compounds with Co(II) and Ni(II), X-ray powder diffraction analysis indicated that the three compounds are isomorphous. IR, UV-VIS and TG data were also consistent with this latter point. Thus, while the isothiocyanate acts as a terminal ligand in these compounds, the bpa ligand has been observed to perform as an efficient spacer giving rise to 1-D complexes. The thermal variation of the magnetic susceptibility for the three compounds has been interpretated in terms of the occurrence of antiferromagnetic coupling between metal ions along with some other effects. However, the theoretical treatment of the experimental data revealed that these interactions are weak, in accordance with the long pathway through the voluminous bpa ligand.

Acknowledgements

This work has been carried out with the financial support of the Universidad del País Vasco/Euskal Herriko Unibertsitatea (Project UPV 130.310.EB234/95) and the Gobierno Vasco/Eusko Jaurlaritza (Project PI96/39). M. L. H. also thanks the Universidad del País Vasco/Euskal Herriko Unibertsitatea for the grant UPV 130.310.EB234/95.

References

1 M. M. Turnbull, T. Sugimoto and L. K. Thompson, *Molecule-Based Magnetic Materials*, American Chemical Society, Washington, DC, 1996.
2 O. Kahn, *Molecular Magnetism*, VCH, Weinheim, 1993.
3 S. M. Kuang, Z. Z. Zhang, Q. G. Wang and T. C. W. Mak, *J. Chem. Soc.*, *Dalton Trans.*, 1997, 4457.
4 R. Cortés, M. Drillon, X. Solans, L. Lezama and T. Rojo, *Inorg. Chem.*, 1997, **36**, 677.
5 M. L. Tong, X. M. Chen, X. L. Yu and T. C. W. Mak, *J. Chem. Soc.*, *Dalton Trans.*, 1998, 5.
6 A. J. Blake, S. J. Hill, P. Hubberstey and W. S. Li, *J. Chem. Soc.*, *Dalton Trans.*, 1998, 909.
7 T. O. S. Jung, S. H. Park, D. C. Kim and K. M. Lim, *Inorg. Chem.*, 1998, **37**, 610.
8 L. Carlucci, G. Ciani, D. M. Proserpio and A. J. Sironi, *J. Chem. Soc.*, *Dalton Trans.*, 1997, 1801.
9 M. Kondo, T. Yoshitomi, K. Seki, H. Matzusaka and S. Kitagawa, *Angew. Chem.*, *Int. Ed. Engl.*, 1997, **36**, 1725.
10 A. J. Blake, N. R. Champness, A. Khlobystov, D. A. Lemenovskii, W. S. Li and M. Schröder, *Chem. Commun.*, 1997, 2027.
11 R. Cortés, M. K. Urtiaga, L. Lezama, J. L. Pizarro, M. I. Arriortua and T. Rojo, *Inorg. Chem.*, 1997, **36**, 5016.
12 T. L. Hennigar, D. C. MacQuarrie, P. Losier, R. D. Rogers and M. J. Zaworotko, *Angew. Chem.*, *Int. Ed. Engl.*, 1997, **36**, 972.
13 K. N. Power, T. L. Hennigar and M. J. Zaworotko, *Chem. Commun.*, 1998, 595.
14 M. Fujita, Y. K. Kwon, M. Miyazawa and K. Ogura, *J. Chem. Soc.*, *Chem. Commun.*, 1994, 1977.
15 J. Lu, T. Paliwala. S. C. Lim, C. Yu, T. Niu and A. J. Jacobson, *Inorg. Chem.*, 1997, **36**, 923.
16 G. M. Sheldrick, SHELXS86, Program for the Solution of Crystal Structures, University of Göttingen, 1985.
17 G. M. Sheldrick, SHELXL93, Program for the Refinement of Crystal Structures, University of Göttingen, 1993.
18 *International Tables for X-ray Crystallography*, Kynoch Press, Birmingham, 1974, vol. IV.
19 J. Rodriguez Carvajal, FULLPROF, Program Rietveld Pattern Matching Analysis of Powder Patterns, 1997.
20 H. M. Rietveld, *Acta Crystallogr.*, 1967, **12**, 151.
21 H. M. Rietveld, *J. Appl. Crystallogr.*, 1969, **6**, 65.
22 A. B. P. Lever, *Inorganic Electronic Spectroscopy*, Elsevier Science B.V., Amsterdam, 1984.
23 V. L. Goedken and D. H. Busch, *J. Am. Chem. Soc.*, 1972, **94**, 7355.
24 A. Abragam and M. H. L. Pryce, *Proc. R. Soc.* (*London*) *A*, 1951, **206**, 173.
25 F. E. Mabbs and D. J. Machin, *Magnetism in Transition Metal Complexes*, Chapman and Hall, London, 1973.
26 M. E. Fisher, *Am. J. Phys.*, 1964, **32**, 343.
27 P. Gütlich, A. Hauser and H. Spiering, *Angew. Chem.*, *Int. Ed. Engl.*, 1994, **33**, 2024.
28 H. Toftlund, *Coord. Chem. Rev.*, 1989, **94**, 67.
29 G. S. Matouzenko, A. Bousseksou, S. Lecocq, P. J. van Koningsbruggen, M. Perrin, O. Kahn and A. Collet, *Inorg. Chem.*, 1997, **36**, 2975.
30 J. A. Real, E. Andrés, M. C. Muñoz, M. Julve, J. Granier, A. Bousseksou and F. Verret, *Science*, 1995, **268**, 265.
31 J. H. Van Vleck, *The Theory of Electrical and Magnetic Susceptibilities*, Oxford University Press, Oxford, 1932.
32 A. Meyer, A. Gleizes, J. J. Girerd, M. Verdaguer and O. Kahn, *Inorg. Chem.*, 1982, **21**, 1729.
33 C. K. Johnson, ORTEP, Report ORNL-5138, Oak Ridge National Laboratory, Oak Ridge, TN, 1976.

Paper 9/00096H